An effective hyperspectral image retrieval method using integrated spectral and textural features

Zhenfeng Shao and Weixun Zhou
State Key Laboratory for Information Engineering in Surveying, Mapping and Remote Sensing, Wuhan University, Wuhan, China
Qimin Cheng
Department of Electronics and Information Engineering, Huazhong University of Science and Technology, Wuhan, China
Chunyuan Diao
Department of Geography, University at Buffalo, The State University of New York, New York, USA, and
Lei Zhang
State Key Laboratory for Information Engineering in Surveying, Mapping and Remote Sensing, Wuhan University, Wuhan, China

Abstract

Purpose – The purpose of this paper is to improve the retrieval results of hyperspectral image by integrating both spectral and textural features. For this purpose, an improved multiscale opponent representation for hyperspectral texture is proposed to represent the spatial information of the hyperspectral scene.

Design/methodology/approach – In the presented approach, end-member signatures are extracted as spectral features by means of the widely used end-member induction algorithm N-FINDR, and the improved multiscale opponent representation is extracted from the first three principal components of the hyperspectral data based on Gabor filters. Then, the combination similarity between query image and other images in the database is calculated, and the first k more similar images are returned in descending order of the combination similarity.

Findings – Some experiments are calculated using the airborne hyperspectral data of Washington DC Mall. According to the experimental results, the proposed method improves the retrieval results, especially for image categories that have regular textural structures.

Originality/value – The paper presents an effective retrieval method for hyperspectral images.

Keywords Image processing, Spectral analysis

Paper type Research paper

1. Introduction

With the increasing availability of the huge volume of Earth Observation data, remote sensing image retrieval technology has drawn more and more public attention in recent years. Traditionally, metadata, such as sensor type, data acquisition time and geographical position, are commonly used for information retrieval from remote sensing databases (Ferecatu and Boujemaa, 2007). Unfortunately, metadata cannot describe the abundant visual information contained in remote sensing images well. In most applications, people are more concerned with the content of remote sensing images rather than corresponding metadata. In addition, metadata-based retrieval usually requires professional knowledge, which has impeded the development and application of remote sensing image retrieval. In this respect, content-based remote sensing image retrieval (CBRSIR) method is a more desired choice. Ozkan *et al.* (2014) compared three CBRSIR representation methods and gave a performance analysis with some experiments on the publicly available UC Merced dataset.

For CBRSIR method, images are characterized by low-level visual features, which can be extracted using feature extraction algorithms, and images are associated with corresponding feature vectors. Given one query image, relevant images will then be retrieved and returned in the order of ascending or descending similarity calculated through predefined similarity measures. In image retrieval community, CBRSIR methods are mostly exploited on high-resolution images (Yang and Newsam, 2013; Wang *et al.*, 2014) and synthetic aperture radar (SAR) images (Espinoza-Molina and Datcu, 2013).

The current issue and full text archive of this journal is available on Emerald Insight at: **www.emeraldinsight.com/0260-2288.htm**

Sensor Review
35/3 (2015) 274–281

[DOI 10.1108/SR-10-2014-0716]

The authors would like to thank the anonymous reviewers for their comments and suggestions. This work was supported by National Science & Technology Specific Projects [grant number 2012YQ16018505] and National Natural Science Foundation of China [grant number 61172174].

Received 2 October 2014
Revised 9 February 2015
Accepted 24 February 2015

Despite the important progress of CBRSIR, few works have been done on hyperspectral images. In recent years, the Computational Intelligence Group of the University of Basque Country has conducted some works on hyperspectral image retrieval (Grana and Veganzones, 2012; Veganzones and Grana, 2012). Grana and Veganzones (2012) extracted end-members as spectral features by end-member induction algorithms and defined an end–member-based image distance to measure the similarity between two hyperspectral images. Both real and synthetic hyperspectral data were used to validate the proposed hyperspectral image retrieval algorithm. It is shown that the proposed algorithm, based on spectral features, is effective in retrieving hyperspectral images. However, the method takes no consideration of the spatial distribution of end-members. To avoid such deficiency and improve retrieval results, Veganzones and Grana (2012) proposed a spectral – spatial retrieval system, which estimated and introduced the fractional abundances of end-members in similarity measure. Plaza *et al.* (2007) proposed a parallel system for efficient hyperspectral image retrieval.

Though some differences exist among above works, they share similar ideas that end-member signatures extracted from hyperspectral images based on linear mixing model are taken as spectral features in the retrieval system, and the similarity between two images is measured through calculating the distance between corresponding spectral features in a feature space. Nevertheless, due to the phenomena that the same object can have very different spectra, and totally different objects may share similar spectra, some hyperspectral images are still difficult to retrieve, even with high spectral resolution. In hyperspectral image processing techniques, spectral and spatial information are complementary. In some cases, it is even mandatory to integrate them together for some certain applications (Plaza *et al.*, 2009).

To improve the performance of hyperspectral image retrieval, we propose a hyperspectral image retrieval method that integrates spectral and textural features. Specifically, spectral features are extracted by end-member induction algorithm, and textural features are computed from the principal component analysis (PCA) – transformed image with Gabor filters.

2. Feature extraction and similarity measure

In this section, the framework of the proposed retrieval method is illustrated first, and details of feature extraction as well as similarity measures used are then introduced.

2.1 Framework of the proposed method

Figure 1 illustrates the framework of the proposed hyperspectral image retrieval method that mainly includes two parts, feature extraction and similarity measure. Both of these are indispensable functional modules of one CBRSIR system. For feature extraction, spectral and textural features are extracted by means of N-FINDR and Gabor filters, respectively, and two feature databases, including a spectral feature database and a textural feature database, are built. Consequently, each image can be represented by the corresponding features stored in the feature databases through indexing mechanism. For similarity measure, the process can be described briefly as follows:

Figure 1 The framework of the proposed hyperspectral image retrieval method

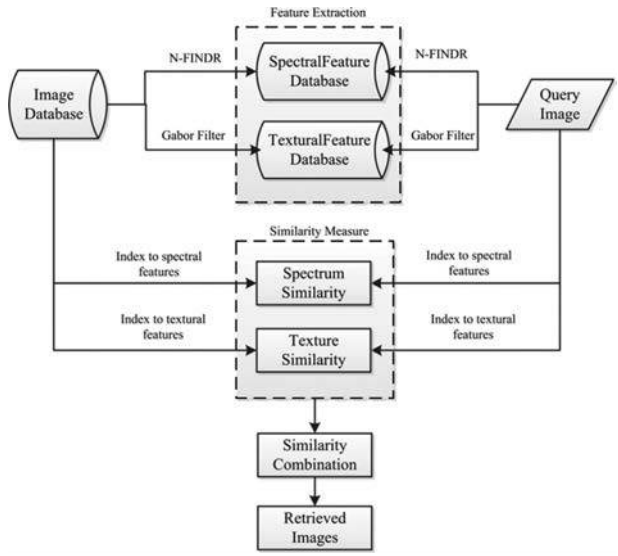

- Calculate the spectrum similarity and the texture similarity between the query image and images in the database through predefined similarity measures.
- Combine the spectrum similarity and the texture similarity, and obtain the combination similarity between these two images.
- Rank the images with descending combination similarity, and return the first k retrieved images.

2.2 Feature extraction procedure

2.2.1 Spectral features

The linear mixing model is widely used for hyperspectral data analysis (Keshava and Mustard, 2002). The core of this model is based on the premise that within a specific hyperspectral scene, the reflectance of each pixel can be described as the linear combination of endmember spectra, and it can be extended to the whole image and denoted by:

$$I = E\Phi + W \tag{1}$$

where I is the hyperspectral image with q spectral bands, $E = [e_1, e_2, \ldots, e_n]$ is a $q \times n$ matrix standing for the end-member signatures of image I and $e_i (i = 1, 2, \ldots, n)$ is one of the extracted end-member signatures of image I. $\Phi = [\varphi_1, \varphi_2, \ldots, \varphi_n]$ is the fractional abundance matrix and $\varphi_i (i = 1, 2, \ldots, n)$ is the fractional abundance vector of end-member e_i. Note that Φ is subject to two constraints: each element of Φ is greater than 0, and the sum of row elements of Φ equals 1. W is the additive noise.

Figure 2(a and b) includes two hyperspectral image patches with the same size, and both have two land cover classes A and B. Assuming the two image patches happen to have the same end-member signatures, then they will be considered very similar through the pre-defined similarity measure. However, in fact, they have low similarity because of the totally different proportions of A and B in each image patch. To overcome such deficiency, the hyperspectral image I can be characterized by the tuple (E, Φ), which takes the spatial

Figure 2 Two hyperspectral image patches with the same land cover classes but totally different proportions

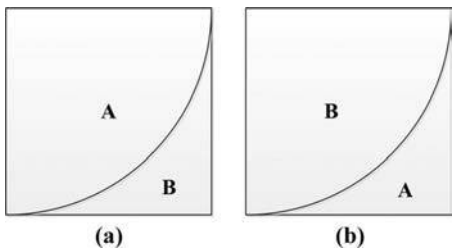

distribution of end-members into consideration, thus improving the retrieval results (Veganzones and Grana, 2012).

Then, the focus of spectral features extraction turns to the extraction of end-member signatures. Many methods have been developed for end-member determination in practice. Veganzones and Grana (2008) gave a comprehensive enumeration of commonly used end-member determination methods, such as N-FINDR (Winter, 1999), Pixel Purity Index) (Boardman *et al.* 1995), Convex Cone Analysis (Ifarraguerri and Chang, 1999) and Automated Morphological Endmember Extraction (Plaza *et al.*, 2002). In the work by Plaza *et al.*(2004), the end-member extraction methods mentioned above and some other methods are rigorously compared by a custom-designed quantitative and comparative framework. However, it is unlikely to find an algorithm that is appropriate for all the situations in end-member extraction. In this article, N-FINDR is used for end-member extraction.

Despite N-FINDR being widely used in various domains, it cannot determine the number of needed end-members (Plaza and Chang, 2005). Here, we provide two strategies to determine the number of induced end-members. The first strategy is to manually assign the number of induced end-members, and the second strategy is to estimate the number of end-members using virtual dimensionality (VD) algorithm (Chang and Du, 2004). We use the package provided by Veganzones and Grana (2012) to implement N-FINDR algorithm based on the two strategies.

In view of the situation that the number of identified and used end-members in practice is ranging from three to seven (Keshava and Mustard, 2002) and the hyperspectral image data used in our experiments contains seven ground cover types, we assign the number of end-members ranging from 3 to 7 for the first strategy.

2.2.2 Textural features

There are various texture representations with respect to texture feature analysis, such as Gabor filter (Manjunath and Ma, 1996), Wavelet Transform (Chang and Kuo, 1993), Local Binary Pattern (LBP) (Ojala *et al.*, 2002) and global morphological texture (Aptoula, 2014). While these texture features tend to achieve ideal performance in image retrieval literature, they are generally designed for processing images with a single band, which are not suitable for multispectral or hyperspectral images directly. Though applying texture extraction methods to each band of the hyperspectral image may be one solution, it suffers from high computational complexity and inefficiency. In addition, each band of the hyperspectral data exhibits nearly the same scene structure, and the information will be redundant if all bands are taken into consideration.

Shi and Healey (2003) proposed a multiscale opponent representation for hyperspectral texture recognition, which is based on Gabor filters and combines spatial information across spectral bands. Motivated by this research, we proposed an improved color texture descriptor for aerial image retrieval in our previous work (Shao *et al.*, 2014). In this paper, the improved color texture descriptor was adapted for hyperspectral texture extraction.

Due to the high dimensionality of hyperspectral data, we present a PCA-based textural feature extraction strategy with lower computational complexity and higher efficiency for hyperspectral data. The following steps illustrate the brief procedures of the proposed strategy.

- Apply PCA to reduce the dimensionality of the whole hyperspectral scene to acquire the first three principal components.
- Partition the principal components into image patches of 32 × 32 pixels size and prepare the retrieval dataset (details can be found in Section 3).
- Extract Gabor opponent (GaborOpp, which is named CGOT in our previous work mentioned above) texture of each image patch and represent each image patch using a GaborOpp feature vector.

Considering that GaborOpp textural feature is fused by Gabor texture and opponent feature, we first introduce the extraction of the two features based on Gabor filters. The Gabor filters used in this paper are as follows (Liu and Wechsler, 2002):

$$\psi_{uv}(z) = \frac{\|k_{uv}\|^2}{\sigma^2} e^{(-\|k_{uv}\|^2 \|z\|^2 / 2\sigma^2)} [e^{ik_{uv}z} - e^{-\sigma^2/2}] \quad (2)$$

where $z = (x, y)$, $u = (0, 1, 2, 3, 4, 5, 6, 7)$ and $v = (0, 1, 2, 3, 4)$ are the orientation and the scale parameters of Gabor kernels. $\|k_{uv}\|$ is the norm operation, and k_{uv} is defined as follows:

$$k_{uv} = k_v e^{i\varphi_u} \quad (3)$$

where $k_v = k_{\max}/f^v$ and $\varphi_u = \pi u/8$. $k_{\max} = \pi/2$ is the maximum frequency, $f = \sqrt{2}$ is the space factor and $\sigma = 2\pi$ denotes the standard deviation.

Let P be an image patch, and $P_i (i = 1, 2, 3)$ be ith principal component of the patch. The convolution of P_i and Gabor kernels ψ_{uv} with orientation u and scale v is given by:

$$g_{iuv}(z) = P_i(z) * \psi_{uv}(z) \quad (4)$$

Gabor texture of each principal component is composed of the mean μ_{uv} and the standard deviation σ_{uv} of the transform coefficients, which are defined by:

$$\begin{cases} \mu_{iuv} = \iint |g_{iuv}(x, y)| \, dxdy \\ \sigma_{iuv} = \sqrt{\iint (|g_{iuv}(x, y)| - \mu_{iuv})^2 dxdy} \end{cases} \quad (5)$$

The Gabor texture of P is characterized by $T = \{\mu_{iuv}, \sigma_{iuv}\}$, which is one 80×3 matrix and ith column represents the textural feature vector of ith principal component.

Let $g_{iuv}(x, y)$ and $g_{juv'}(x, y)$ be the convolution results of different principal components P_i and $P_j(i, j = 1, 2, 3; i \neq j)$, respectively, of image patch P using equation (4), and the normalized difference between $g_{iuv}(x, y)$ and $g_{juv'}(x, y)$ can be defined by:

$$d_{ijuvv'}(x,y) = \frac{g_{iuv}(x,y)}{\sqrt{\sum g^2_{iuv}(x,y)}} - \frac{g_{juv'}(x,y)}{\sqrt{\sum g^2_{juv'}(x,y)}} \quad (6)$$

where u and v, v' denote the orientation and scales of Gabor filters used, respectively. Note that v and v' are adjacent scales, which means they meet the condition $|v - v'| \leq 1$.

Thus, 13 scale groups and 8 orientations are available. In terms of scale groups, they are: $(v,v') \in \{(0,0), (1,1), (2,2), (3,3), (4,4), (0,1), (1,0), (1,2), (2,1), (2,3), (3,2), (3,4), (4,3)\}$. The opponent feature of P can be characterized by $opp = \{\sqrt{\sum d^2_{ijuvv'}(x, y)}\}$, which is a total of 312 feature vectors. Then GaborOpp texture is defined by:

$$GaborOpp = \left\{\mu_{iuv}, \sigma_{iuv}, \sqrt{\sum d^2_{ijuvv'}}\right\} \quad (7)$$

As one of the comparative features, the multiscale opponent representation (UniOpp) used for hyperspectral texture recognition by (Shi and Healey, 2003) can be characterized as:

$$UniOpp = \left\{\sqrt{\sum g^2_{iuv}(x,y)}, \sqrt{\sum d^2_{ijuvv'}(x,y)}\right\} \quad (8)$$

2.2.3 Similarity measures

Effective image similarity measures are requisite for accurate image retrieval. For spectral features, the spectral–spatial dissimilarity measure is used to calculate the dissimilarity between two image patches (Veganzones and Grana, 2012).

Let $E_1 = [e^1_1, e^1_2, \ldots, e^1_m]$ and $E_2 = [e^2_1, e^2_2, \ldots, e^2_n]$ be the end-member signatures of image H_1 and H_2, respectively, where m and n are the number of end-members. Define $D_{12} = [d_{ij}; i = 1, 2, \ldots, m; j = 1, 2, \ldots, n]$ as the end-member distance matrix, and d_{ij} as the distance between the end-member pair from E_1 and E_2. In this article, d_{ij} is calculated by means of spectral angle mapper, one common distance metric in hyperspectral image processing as follows:

$$d_{ij} = \arccos\left(\frac{<\boldsymbol{e}^1_i, \boldsymbol{e}^2_j>}{\|\boldsymbol{e}^1_i\|\|\boldsymbol{e}^2_j\|}\right) \quad (9)$$

where e^1_i and e^2_j are the end-member vectors of E_1 and E_2, respectively. The spectrum dissimilarity between H_1 and H_2 is given by:

$$D^S(H_1, H_2) = \sum_{i,j} r_{ij} d_{ij} \quad (10)$$

where d_{ij} is the spectral distance between two end-members from E_1 and E_2, and r_{ij} is the significance matrix associated with d_{ij}. The readers can refer to the work by Veganzones and Grana (2012) for more details about the computation of the significance matrix r_{ij}.

For GaborOpp textural feature, the texture dissimilarity between H_1 and H_2 is given by:

$$D^T(H_1, H_2) = \sum_{i=1}^{p}\left(\left|\frac{f^i_1 - f^i_2}{\sigma^i}\right|\right) \quad (11)$$

where $f^i_1(i = 1, 2, \ldots, p)$ and $f^i_2(i = 1, 2, \ldots, p)$ are corresponding elements of GaborOpp texture vector of image H_1 and H_2, respectively, and $\sigma^i(i = 1, 2, \ldots, p)$ is the standard deviation of GaborOpp texture over the entire image database.

The combination dissimilarity $D^C(H_1, H_2)$ between H_1 and H_2 is defined by:

$$D^C(H_1, H_2) = \alpha D^S(H_1, H_2) + \beta D^T(H_1, H_2) \quad (12)$$

where $D^S(H_1, H_2)$ and $D^T(H_1, H_2)$ are spectrum dissimilarity and texture dissimilarity, respectively. α and β are the weight of spectrum dissimilarity and texture dissimilarity in the combination similarity, respectively, and can be determined by:

$$\begin{cases}\alpha + \beta = 1 \\ \alpha - \beta = D^S(H_1, H_2) - D^T(H_1, H_2)\end{cases} \quad (13)$$

3. Experiments and analysis

The airborne hyperspectral data of Washington DC Mall is used to evaluate the performance of the proposed method. The original hyperspectral cube has 210 bands in 0.4- to 2.4-μm region, but only 191 bands are commonly used. The bands in 0.9- and 1.4-μm regions are omitted because the atmosphere is opaque. Consequently, the data cube used in our experiments has 1,208 lines, 307 samples and 191 bands.

The scene of Washington DC Mall is partitioned into 314 image patches of 32 × 32 pixels size. Image patches with similar scenes are manually grouped into one category. Figure 3 gives five example patches of per category. The name and number of each category are (Figure 3(a)) Grass-24, (Figure 3(b)) Road-60, (Figure 3(c)) Mixture-20 (including three land cover types, grass, tree and trail), (Figure 3(d)) Others-44 (including more land cover types, such as grass, building, road and tree), (Figure 3(e)) Tree-42, (Figure 3(f)) Water-24 and (Figure 3(g)) Building-100. Thus, the retrieval database is challenging for image retrieval because it contains various land cover types. Note that if an image patch is mainly dominated by a specific image class, then it will be grouped into this category, such as Grass, Road, Tree, Water and Building. However, if it is difficult to determine the dominated image class of an image patch, then it will be grouped into either Mixture or Others.

3.1 Experiment I

This section describes the performance of spectral features using the two abovementioned strategies to determine the number of induced end-members. Table I shows the retrieval precision of each category using spectral features based on the two strategies. It is interesting that the best performance of each category results from various number of end-members. It indicates that the number of end-members or, in other words,

Figure 3 Five image patches per category of the retrieval database

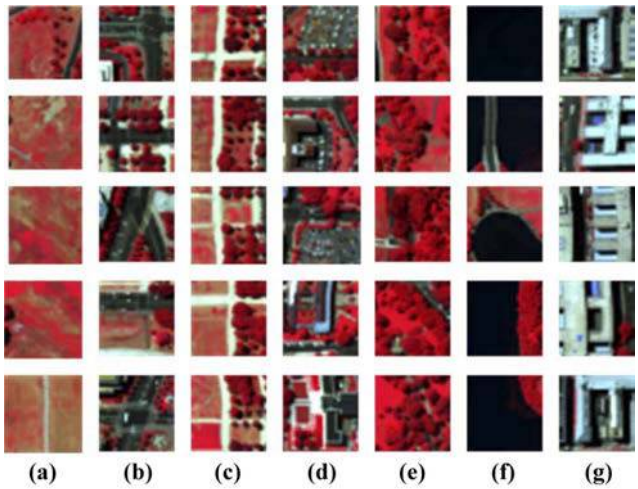

Notes: (a) Grass; (b) Road; (c) Mixture; (d) Others; (e) Tree; (f) Water; and (g) Building

Table I Retrieval precision of each category using spectral features with two strategies to determine the number of induced end-members

Category	VD	3	4	5	6	7
Grass	0.5533	0.3187	0.5278	0.4952	0.4925	0.5071
Road	0.3827	0.2724	0.3223	0.3393	0.3608	0.4137
Mixture	0.3444	0.3860	0.3201	0.3819	0.2849	0.3191
Others	0.2511	0.2393	0.2877	0.2997	0.2862	0.2558
Tree	0.4426	0.3115	0.4214	0.3732	0.3612	0.3702
Water	0.7115	0.7462	0.8149	0.7716	0.7387	0.7208
Building	0.6194	0.5202	0.5514	0.5938	0.6871	0.6368

the strategy used to determine the number of needed end-members is an important factor that affects the spectral retrieval result. To reduce this impact and improve the performance, an improved strategy (IS) is proposed and briefly described as follows. For the categories Grass and Tree, VD is used to estimate the number of induced end-members. For the categories Mixture, Water, Others, Building and Road, the number of induced end-members is assigned 3, 4, 5, 6 and 7, respectively. Estimating the number of needed end-members is still an open question in spectral unmixing literature, but it is not the focus of our work in this paper. Therefore, we call IS "strategy" rather than "method" here, which means IS is introduced to decrease the influence of the number of end-members on the retrieval performance to some extent, and it is not appropriate for other applications as VD algorithm does.

The average precision of each category using above strategies to determine the number of needed end-members is shown in Figure 4. It is apparent that IS improves the retrieval performance of the categories Mixture, Others and Water, and it achieves higher precision than most of the other methods for the categories Grass, Road, Tree and Building. The last bin shows the precision averaged over all image categories. We can see that the best performance results from the IS. This makes sense because the spectral features with appropriate number of

Figure 4 Average precision of each category with various numbers of endmembers

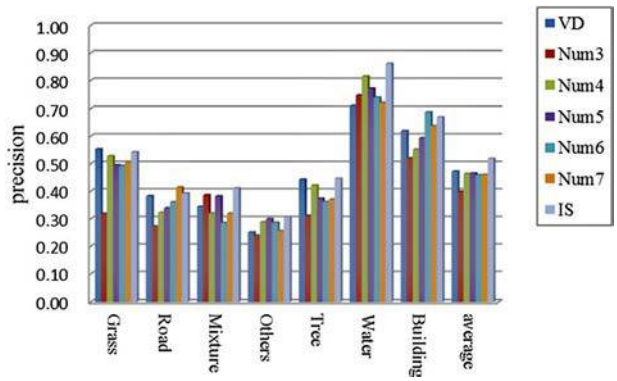

end-members provide a better representation of the hyperspectral scene.

In subsequent experiments, IS is applied to determine the number of induced end-members.

3.2 Experiment II

Despite the good performance of spectral features for some image classes, the overall performance measured by average precision is not satisfying. In addition, those image categories that have regular textural structures, such as Grass, Road and Mixture, have not achieved better performance as expected. From this respect, the image retrieval system should benefit from the incorporation of textural information.

Table II summarizes the performance of GaborOpp texture against three comparative features. For Gabor texture and UniOpp texture, Section 2.2.2 shows the detailed process of feature extraction. For LBP feature, we compute $LBP^{riu2}_{8,1}$, which means LBP has been implemented using 8 pixels circular neighbor of radius 1 in our experiments. According to the results in Table II, GaborOpp has better performance on the hyperspectral dataset than the other three texture features, indicating the powerful representation performance of GaborOpp texture.

Table III demonstrates the advantage of hyperspectral image retrieval using integrated spectral and GaborOpp features. For the categories Grass, Road and Mixture, integrated features improve the performance dramatically compared with spectral features. For the categories Others, Tree, Water and Building, which have no obviously regular

Table II The performance of the improved texture feature against other texture features

Category	GaborOpp	Gabor	UniOpp	LBP
Grass	0.7396	0.8026	0.6789	0.3617
Road	0.4217	0.3922	0.4056	0.3286
Mixture	0.8418	0.6079	0.8284	0.4069
Others	0.3134	0.2958	0.3071	0.2855
Tree	0.5671	0.5187	0.5657	0.3534
Water	0.6962	0.7607	0.6201	0.6141
Building	0.5959	0.6147	0.5864	0.5095
Average	0.5965	0.5704	0.5703	0.4085

Table III Retrieval result of each category using spectral features, GaborOpp textural features and integrated features

Category	Spectral features	GaborOpp	Integrated features
Grass	0.4529	0.7396	0.7443
Road	0.3933	0.4217	0.5046
Mixture	0.4299	0.8418	0.8591
Others	0.2931	0.3134	0.3450
Tree	0.5330	0.5671	0.5784
Water	0.8762	0.6962	0.8246
Building	0.7301	0.5959	0.7450
Average	0.5298	0.5965	0.6573

textural structures, integrated features have similar performance as spectral features indicating that textural features are valuable information for hyperspectral image retrieval, particularly for those categories having regular textural structures.

The precision-recall curve is used to further evaluate the performance of integrated features. Postulating a query that searches for the first k more similar images to the query image, then precision is defined as the fraction of relevant images in k retrieved images and recall is defined as the fraction of relevant images that are retrieved in the entire image database. The precision-recall curve for spectral features, textural features and integrated features is shown in Figure 5. The plots demonstrate that the integrated features outperform spectral features and textural features. In terms of textural features, the improved color texture descriptor GaborOpp has better performance compared to the other three textural features. However, when recall is greater than 0.45, the curve of integrated features decreases quickly. Two reasons can be used to explain this phenomenon. On one hand, retrieving the first k more relevant images becomes more difficult when the query scope k increases, and the complexity of the image scenes compromises the performance. On the other hand, the number of images of each category is uneven. So as the query scope k increases, the proportion of relevant images in the returned images is down rapidly for the categories of small size, and is down slowly for the categories of big size.

The results shown in Figure 5 not only demonstrate the advantages of the integrated features for hyperspectral image retrieval but also provide the insight that the number of images of each category should be as even as possible. In addition, the idea that textural features incorporating discriminative information among color bands have better representation performance may be informative for other applications such as texture recognition and classification.

Figure 5 The precision-recall curves for spectral features, textural features and integrated features

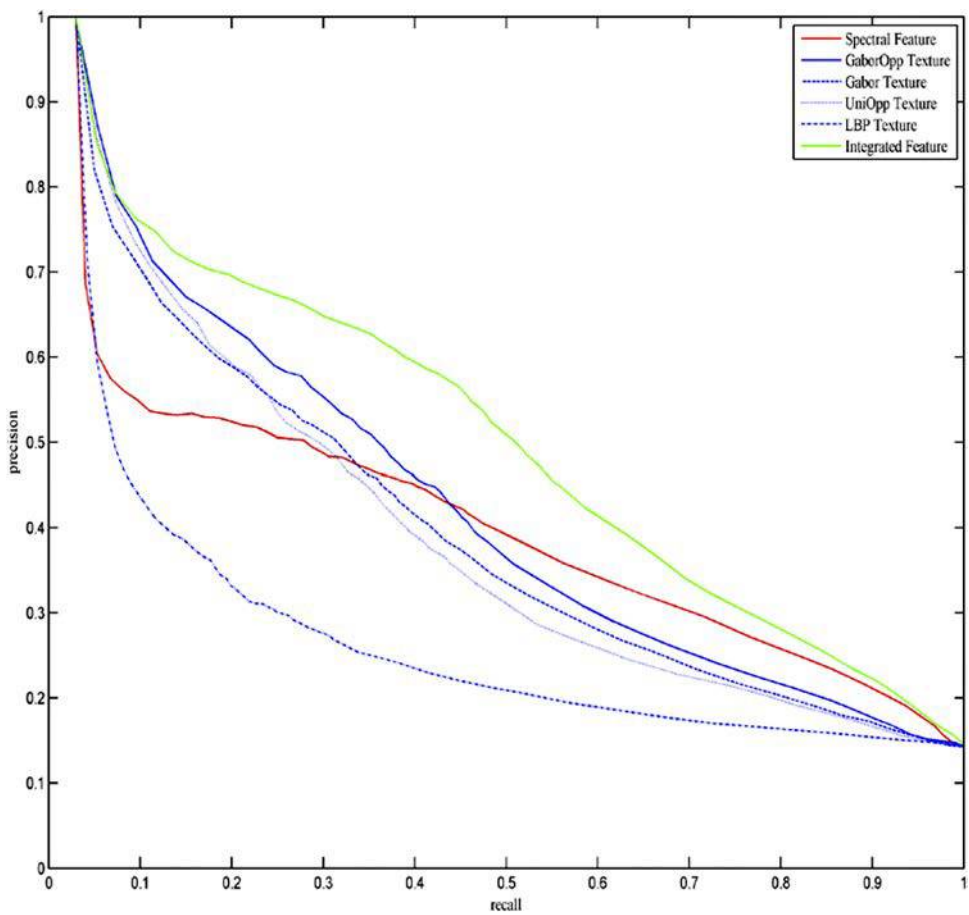

4. Conclusion and future work

We present an effective retrieval method that integrates spectral and textural features for hyperspectral images. For spectral features, we introduce three strategies to estimate the number of needed end-members when using N-FINDR to extract the end-members. For textural features, we propose an improved color texture descriptor that has been demonstrated to be effective for hyperspectral image retrieval. The experiments show that integrated features outperform spectral features measured by several performance metrics. In addition, the experiments also indicate that textural features can be used as complementary information for hyperspectral image retrieval, particularly for image categories that have regular textural structures.

In future, a more powerful end-member determination strategy allowing for different image categories will be studied, and integration of semantic features to bridge the semantic gap will be considered as well.

References

Aptoula, E. (2014), "Remote sensing image retrieval with global morphological texture descriptors", *IEEE Transactions on Geoscience and Remote Sensing*, Vol. 52 No. 5, pp. 3023-3034.

Boardman, J.W., Kruse, F.A. and Green, R.O. (1995), "Mapping target signatures via partial unmixing of AVIRIS data", *In Summaries of the VI JPL Airborne Earth Science Workshop*, Pasadena, CA.

Chang, C.I. and Du, Q. (2004), "Estimation of number of spectrally distinct signal sources in hyperspectral imagery", *IEEE Transactions on Geoscience and Remote Sensing*, Vol. 42 No. 3, pp. 608-619.

Chang, T. and Kuo, C.C. (1993), "Texture analysis and classification with tree-structured wavelet transform", *IEEE Transactions on Image Processing*, Vol. 2 No. 4, pp. 429-441.

Espinoza-Molina, D. and Datcu, M. (2013), "Earth-observation image retrieval based on content, semantics, and metadata", *IEEE Transactions on Geoscience and Remote Sensing*, Vol. 51 No. 11, pp. 5145-5159.

Ferecatu, M. and Boujemaa, N. (2007), "Interactive remote-sensing image retrieval using active relevance feedback", *IEEE Transactions on Geoscience and Remote Sensing*, Vol. 45 No. 4, pp. 818-826.

Grana, M. and Veganzones, M.A. (2012), "An endmember-based distance for content based hyperspectral image retrieval", *Pattern Recognition*, Vol. 45 No. 9, pp. 3472-3489.

Ifarraguerri, A. and Chang, C.I. (1999), "Multispectral and hyperspectral image analysis with convex cones", *IEEE Transactions on Geoscience and Remote Sensing*, Vol. 37 No. 2, pp. 756-770.

Keshava, N. and Mustard, J.F. (2002), "Spectral unmixing", *IEEE Signal Processing Magazine*, Vol. 19 No. 1, pp. 44-57.

Liu, C. and Wechsler, H. (2002), "Gabor feature based classification using the enhanced fisher linear discriminant model for face recognition", *IEEE Transactions on Image Processing*, Vol. 11 No. 4, pp. 467-476.

Manjunath, B.S. and Ma, W.Y. (1996), "Texture features for browsing and retrieval of image data", *IEEE Transactions on Pattern Analysis and Machine Intelligence*, Vol. 18 No. 8, pp. 837-842.

Ojala, T., Pietikainen, M. and Maenpaa, T. (2002), "Multiresolution gray-scale and rotation invariant texture classification with local binary patterns", *IEEE Transactions on Pattern Analysis and Machine Intelligence*, Vol. 24 No. 7, pp. 971-987.

Ozkan, S., Ates, T., Tola, E., Soysal, M. and Esen, E. (2014), "Performance analysis of state-of-the-art representation methods for geographical image retrieval and categorization", *IEEE Geoscience and Remote Sensing Letters*, Vol. 11 No. 11, pp. 1996-2000.

Plaza, A., Benediktssonb, J.A., Boardmanc, J.W., Braziled, J., Bruzzonee, L., Camps-Vallsf, G., Chanussotg, J., Fauvelg, M., Gambah, P., Gualtierii, A., Marconcinie, M., Tiltoni, J.C. and Triannih, G. (2009), "Recent advances in techniques for hyperspectral image processing", *Remote Sensing of Environment*, Vol. 113 No. S1, pp. S110-S122.

Plaza, A. and Chang, C.I. (2005), "An improved N-FINDR algorithm in implementation", *Proceeding SPIE 5806, Algorithms and Technologies for Multispectral, Hyperspectral, and Ultraspectral Imagery XI*, SPIE, *Orlando, Bellingham*, pp. 298-306.

Plaza, A., Martinez, P., Pérez, R. and Plaza, J. (2002), "Spatial/spectral endmember extraction by multidimensional morphological operations", *IEEE Transactions on Geoscience and Remote Sensing*, Vol. 40 No. 9, pp. 2025-2041.

Plaza, A., Martínez, P., Pérez, R. and Plaza, J. (2004), "A quantitative and comparative analysis of endmember extraction algorithms from hyperspectral data", *IEEE Transactions on Geoscience and Remote Sensing*, Vol. 42 No. 3, pp. 650-663.

Plaza, A., Plaza, J., Paz, A. and Blazquez, S. (2007), "Parallel CBIR system for efficient hyperspectral image retrieval from heterogeneous networks of workstations", *9th International Symposium on Symbolic and Numeric Algorithms for Scientific Computing*, IEEE, Timisoara, NJ, pp. 285-291.

Shao, Z., Zhou, W., Zhang, L. and Hou, J. (2014), "Improved color texture descriptors for remote sensing image retrieval", *Journal of Applied Remote Sensing*, Vol. 8 No. 1, pp. 083584-083584.

Shi, M. and Healey, G. (2003), "Hyperspectral texture recognition using a multiscale opponent representation", *IEEE Transactions on Geoscience and Remote Sensing*, Vol. 41 No. 5, pp. 1090-1095.

Veganzones, M.A. and Grana, M. (2008), "Endmember extraction methods: a short review", *12th International Conference on Knowledge-Based Intelligent Information and Engineering Systems*, Springer, Zagreb, Berlin, pp. 400-407.

Veganzones, M.A. and Graña, M. (2012), "A spectral/spatial CBIR system for hyperspectral images", *IEEE Journal of*

Selected Topics in Applied Earth Observations and Remote Sensing, Vol. 5 No. 2, pp. 488-500.

Wang, X., Shao, Z., Zhou, X. and Liu, J. (2014), "A novel remote sensing image retrieval method based on visual salient point features", *Sensor Review*, Vol. 34 No. 4, pp. 349-359.

Winter, M.E. (1999), "N-FINDR: an algorithm for fast autonomous spectral end-member determination in hyperspectral data", *Proceeding SPIE 3753, Imaging Spectrometry V, SPIE, Denver, Bellingham*, pp. 266-275.

Yang, Y. and Newsam, S. (2013), "Geographic image retrieval using local invariant features", *IEEE Transactions on Geoscience and Remote Sensing*, Vol. 51 No. 2, pp. 818-832.

Corresponding author

Weixun Zhou can be contacted at: weixunzhou1990@whu.edu.cn